Defects and inhomogeneities in Fe$_3$O$_4$(111) thin film growth on Pt(111)

A. Sala, H. Marchetto, Z.-H. Qin, S. Shaikhutdinov, Th. Schmidt, and H.-J. Freund

Fritz Haber Institute of the Max Planck Society, Department of Chemical Physics, Faradayweg 4-6, D-14195 Berlin, Germany

Growth and surface termination of a Fe$_3$O$_4$(111) thin film on a Pt(111) surface were examined by a combination of low-energy electron microscopy, selected area low-energy electron diffraction (LEED), and x-ray-induced photoemission electron microscopy. The film exhibits the predominance of one out of two possible rotational domains, independent of film thickness. The morphology strongly depends on preparation conditions, e.g., at high oxidation temperature FeO/Pt(111) domains are formed that prevent the closure of the thin film. Dynamical LEED analysis and spot-profile analysis LEED (SPA-LEED) show that the surface exposes $\frac{1}{4}$ monolayer of Fe over a close-packed oxygen layer only when the sample is subsequently annealed in ultrahigh vacuum at 900 K. In contrast, the as-prepared films grown by oxidation at 1000 K and subsequent cooling down in oxygen, additionally exhibit small FeO$_x$ agglomerates that rest upon the canonical surface termination. Their formation as a function of the various preparation conditions of the thin film is discussed.

I. INTRODUCTION

Iron oxides are transition-metal compounds with a wide range of technical applications and have, therefore, been studied extensively. In particular, Fe$_3$O$_4$ (magnetite) has been investigated with respect to heterogeneous catalysis,[1,2] magnetism,[3,4] and other fields of research. Many of the functional properties of iron oxides are connected to surface structures. Despite intense and detailed investigation in the last two decades,[5,6] still some important aspects are under controversial debate, mainly regarding the strong dependence on the surface preparation, e.g., using (i) a single crystal instead of a thin film grown on a crystalline support, (ii) different oxidation temperatures, and/or (iii) oxygen partial pressures. As a short overview of the various structural models proposed up to now, we cite first of all the low-energy electron diffraction (LEED) analyses of Barbieri *et al.*[7] and Ritter and Weiss,[8] who find the 1/4 monolayer (ML) of Fe over a close-packed O layer as the most favored atomic termination of a Fe$_3$O$_4$(111) thin film grown on a Pt(111) surface. However, temperature programmed desorption (TPD), infrared reflection absorption spectroscopy (IRAS), and high resolution electron energy loss spectroscopy (HREELS) studies of adsorbed CO as a probe molecule suggest a surface terminated by 1/2 ML of iron.[9] Condon *et al.*[10] with scanning tunneling microscopy (STM) and LEED observed the formation of the so-called "biphase" surface at low oxidation temperatures on Fe$_3$O$_4$(111) single crystals. This was, also, found on magnetite thin films grown on Pt(111) by Shaikhutdinov *et al.*[11] Shvets *et al.* suggested the formation of an O-terminated surface with superperiodic features when a Fe$_3$O$_4$(111) single crystal is cooled down after oxidation while maintaining the oxygen exposure.[12] Such variability in the surface structure may only be understood via a more systematic and comprehensive study of the various parameters that influence the preparation process. The knowledge of the effects of the different preparation parameters is crucial for a correct comparison of the existing results, for merging them into a clear and unambiguous global picture, and for tailoring the film properties, depending on the goal of future experiments. Moreover, modifications in the preparation recipe could lead to improved surface structure, morphology, and do-

main structure of the magnetite thin film as well as the related physical properties, such as magnetic properties, chemical reactivity, and nucleation and encapsulation of nanoparticles.[13]

The present work aims at studying the growth and surface termination of a Fe$_3$O$_4$(111) thin film on a Pt(111) surface, with a focus on the effects of preparation parameters such as oxidation and annealing temperature and morphology of the metal substrate. The Fe$_3$O$_4$(111) films have previously been investigated by using STM, LEED, x-ray photoelectron spectroscopy (XPS),[14] and low-energy electron microscopy (LEEM).[4,15] Our approach is based on the capabilities of a special electron microscope called SMART, the energy-filtered aberration-corrected LEEM/photoemission electron microscopy (PEEM) operating at BESSY II, the synchrotron radiation facility of the Helmholtz Zentrum Berlin. This spectro-microscope combines spectroscopy [electron-energy-loss spectroscopy (EELS), XPS, ultraviolet photoemission spectroscopy (UPS), and near-edge x-ray absorption fine structure (NEXAFS)], microscopy [LEEM, UV-PEEM, and x-ray-induced photoemission electron microscopy (XPEEM)], and diffraction techniques [LEED, x-ray photoelectron diffraction (XPD), and valence-band mapping] to obtain spatially resolved information about, e.g., morphology, chemical distribution, work function, and structural properties, and to perform spectroscopy and diffraction from small object areas.[16] The demonstrated lateral resolution of 2.6 nm[17] and the possibility to record images in video rate allow us to study not only the "static" thin film surface, but also the formation of the thin film itself, by observing *in situ* and *in real time* the surface during the Fe deposition and the oxidation, both on nanoscopic and mesoscopic scale and under variable sample temperatures and O$_2$ pressures.[18]

II. EXPERIMENT

The specimen chamber of SMART with a base pressure of 1×10^{-10} mbar operates from ultrahigh vacuum (UHV) up to a high vacuum regime of 1×10^{-5} mbar of oxygen atmosphere. The Pt(111) crystal has been mounted on a commercial ELMITEC sample holder with a Mo cap. The sample was heated from the back side by radiation from a

filament for T < 700 K or by electron bombardment for T > 700 K with a possible maximum temperature of 2000 K. The temperature was measured with an accuracy better than 10 K by a W26%Re/W5%Re thermocouple spot-welded to the crystal support. Oxygen (99.999% purity) was dosed by a leak valve directly into the specimen chamber of the microscope. The Fe evaporator (Omicron EFM3 with an iron rod of 99.995% purity, Alfa Aesar) pointed toward the sample under grazing incidence angle of $20°$.

For imaging, SMART uses either reflected [LEEM or mirror electron microscopy (MEM)] or photoemitted (PEEM, XPEEM) electrons. In the LEEM mode, an electron gun illuminates the sample surface with a parallel beam of typically 20 μm in diameter. The kinetic electron energy at the sample surface can be set in the range between 0 and 1000 eV. The diffracted electrons are directly imaged through a system of magnetic and electrostatic lenses on a two-dimensional (2D) detector, where the magnified electron image of the surface can be observed in video rate. By changing the kinetic energy, the wavelength, and therefore the diffraction condition, can be optimized to enlarge the image contrast. In this way, monoatomic steps appear as dark lines or areas with different crystal structure differ in intensity. One distinguishes between imaging the specularly reflected electrons (so-called bright-field imaging) and using nonspecularly reflected electrons of a diffraction spot (dark-field imaging). With the latter, superstructure domains or domains with rotated crystalline orientation (texture) can be identified. The electrons can be filtered in energy by a special omega-shaped magnetic imaging analyzer. In this experiment the energy bandwidth has been set to 0.5 eV in order to cut off the inelastically scattered electrons and the secondaries.

The Pt(111) surface was cleaned by cycles of argon sputtering and UHV annealing at 1100 K and with an O_2 treatment $(1 \times 10^{-6}$ mbar, 700 K) to remove carbon contamination followed by UHV annealing up to 1200 K. This yielded a sharp LEED pattern without a structured background. The LEEM imaging showed smooth surface areas with terraces partially more than 1 μm wide, separated by a bunch of some tens of atomic steps.

III. RESULTS

Fe_3O_4(111) thin films are formed by repeated cycles of Fe deposition at room temperature and oxidation at elevated temperatures, where in a first step one complete layer of FeO on the Pt(111) surface was produced, and subsequently an up to 10-nm-thick Fe_3O_4 film was grown.[5]

A. Growth and morphology of the iron oxide film

1. The initial FeO layer

The real-time observation of Fe deposition and subsequent oxidation in LEEM provides access to many details during the formation of the thin oxide film. Above room temperature, the growth of Fe that aggregates on the Pt(111) surface followed a Volmer-Weber mode, with the size and the density of three-dimensional (3D) islands strongly depending on the substrate temperature.[19] At 300 K, deposition of 1 ML of Fe resulted in uniformly distributed islands with a width below 20

nm, almost fully ($\sim$80%) covering the Pt substrate. In contrast, at slightly elevated temperatures of 350 K, the number of islands was considerably lower, the lateral island size clearly enlarged to several hundreds of nanometers, its shape was now triangular, and the height increased, as estimated from the deposited amount, the density and the lateral size. This change in morphology was driven by diffusion as the effect is enhanced at higher temperature. This means that thermodynamically Fe does not wet the Pt(111) surface. This tendency to dewet the surface can only be overcome by decreasing the temperature in order to reduce diffusion, as it is already known for other systems [for example, Pb/Si(111)[20] or Pb/Cu(111)].[21] In this respect, the Pt(111) substrate shows a behavior opposite to Ru(0001), investigated by Monti *et al.* with LEEM.[15] Here, the first Fe layer is completely wetting the substrate at 520 K, documented by the merging of large 2D islands into a closed film.

In the case of the Pt(111) substrate, the morphology of the first Fe layer strongly influences the subsequent formation of a FeO(111) layer. The Fe film was oxidized at 1×10^{-6} mbar of O_2, starting at room temperature, followed by annealing with a rate below 10 K/s up to finally 1000 K, which was kept for 2 min. Upon cooling, the oxygen pressure was reduced not before reaching 500 K. During the annealing in oxygen, the contrast in the LEEM image changed at 820 K, corresponding to a significant change in the film structure. This oxygen treatment produced a complete FeO(111) film covering the entire Pt substrate—but only if iron was initially deposited at 300 K. Starting, however, with a dewetted Fe film, i.e., isolated 3D Fe islands grown at 350 K, the same oxygen treatment led to an incomplete FeO(111) film with well isolated iron oxide islands. This, probably, is related to a different morphology of the deposited Fe on the substrate, as well as some Fe depletion due to the migration of a fractional amount of Fe into the Pt(111) substrate, enabled by the higher deposition temperature.[22]

The Fe deposition rate was calibrated using LEEM *in situ* and *in real time*: here 1 ML of Fe is defined as the amount deposited at 300 K that leads to a perfectly closed FeO(111) layer after oxidation. For Fe amounts slightly larger than 1 ML, the material in excess formed well-ordered FeO_x islands of triangular or hexagonal shape,[23] which could be easily distinguished from the first FeO(111) layer by a different reflectivity of the electron beam at specific kinetic energies (i.e., 3 eV). The structural quality of the FeO(111) single layer was evaluated by LEED, yielding results comparable to those reported in Ref. 8.

2. The Fe_3O_4(111) thin film

The Fe_3O_4(111) film was grown by cycles of subsequent Fe deposition and oxidation. Per cycle, a larger amount of Fe (between 5 and 10 ML) was deposited on a complete FeO(111) film at a substrate temperature below 350 K. During Fe deposition, the intensity of the LEEM image gradually decreased, and the step contrast slightly changed, but the image contrast of the substrate morphology, caused by atomic steps and step bunches, remained unchanged. This can be explained by the formation of rough Fe islands with dimensions smaller than the lateral resolution in this experiment (<20 nm). The amount of the deposited material per cycle was varied between
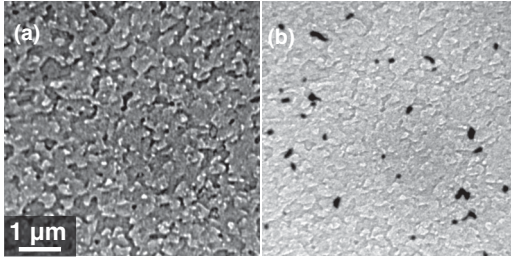
FIG. 1. Example of a well-prepared Fe_3O_4 film, completely covering the Pt(111) substrate. (a) Wide-range bright-field and (b) dark-field LEEM images of the identical surface area using the (0;0) and (1/2;0) spot, respectively. The contrast is due to the film morphology. Additionally, the domains rotated by 180° become visible as dark areas in the dark-field image. Image (a) is in slight overfocus to enhance the contrast, the electron energy $E_{Kin} = 24$ eV in both images.

5 and 10 ML, with no appreciable difference in the quality of the resulting oxide films. The oxidation procedure was the same as described above for FeO, but the final oxidation temperature was reduced to 900 K and kept for 5 min. By following this procedure, we succeeded to produce Fe_3O_4 films, completely covering the entire sample [Fig. 1(a)]. The LEED pattern of the film matched perfectly the one described in Ref. 5. The film consists of terraces up to a width of 100 nm, and most of them with polygonal shape. According to LEEM, the step density increased after every cycle, especially above 20 nm of film thickness. The film could, however, be smoothed if the last oxidation treatment was performed at a slightly elevated temperature of ∼1000 K. For this temperature treatment, it was necessary that the film was completely closed and thicker than 7 nm; otherwise, the annealing up to 1000 K led to a dewetting (see Sec. III C). A subsequent thermal flash in UHV did not produce further morphological changes but improved the homogeneity of the surface structure (see Sec. III D).

B. Crystallographic inhomogeneities

Magnetite crystallizes in an inverse spinel structure with space group $Fd3m$, while the Pt substrate exhibits a fcc structure with space group $Fm3m$. Therefore, during thin film formation on clean Pt(111), the Fe_3O_4 islands created by initial nucleation can only coalesce with improper stacking[19,24] and form a complete film with two twin domains rotated by 180°. Dark-field LEEM studies using the (1/2;0) and (0;1/2) spots showed an unexpected distribution of rotational domains. For every film completely covering the metal surface we prepared, a predominance of one rotational domain was observed. Depending on the preparation condition the coverage ratio for the rotational domains ranged between 75%/25% and 98%/2%. Figure 1(b) shows a dark-field LEEM image visualizing the two rotational domains as dominating bright and small black areas. This preponderance is maintained even after subsequent cycles of Fe deposition and oxidation. On average, the rotational domain size is larger than the terrace width; some of the domains were even several microns wide. A comparison between dark-field and bright-field LEEM images shows that the rotational domains are preferentially

placed in correspondence of the step bunches of the substrate, providing a partial correlation between substrate morphology and crystallographic inhomogeneities.[25]

C. Morphological inhomogeneities

A crucial parameter for the uniformity of the thin film is the oxidation temperature. On the one hand, it should be high enough to enable the oxidation process, but on the other hand, not too high, especially during the first deposition cycles, to avoid a dewetting of the Fe_3O_4 film. The latter was observed at oxidation temperatures above 900 K, as FeO areas became clearly visible in the "holes" of the Fe_3O_4(111) film. The width of these FeO domains increased dramatically at further increase of the temperature, from approximately 100 nm to several microns for an oxidation temperature of 1000 K. The FeO areas could be identified by various experiments: bright- and dark-field LEEM, LEED, and XPEEM. In the dewetted case, bright-field LEEM images [Fig. 2(a)], Fe_3O_4 (dark) and FeO (white) areas, are visible with different contrast, while the corresponding LEED pattern shows the superposition of the Fe_3O_4(111) pattern and the Moiré pattern [six satellite spots surrounding the central (0;0) spot] typical for the FeO(111)/ Pt(111) interface. By dark-field imaging using the Fe_3O_4 (1/2;0) and (0;1/2) spots [Figs. 2(b) and 2(c)], the FeO areas appear dark, while the Fe_3O_4 areas show a contrast between rotational domains due to the threefold symmetry of the Fe_3O_4(111) crystal structure. On the contrary, the FeO domains can be unambiguously identified as brighter areas if one of the satellite spots around (0;0) is selected [Fig. 2(d)]. XPEEM images obtained with Pt 4 $f_{7/2}$ core level emission line [Fig. 2(e)] additionally reveal that the FeO domains formed by dewetting are indeed deep holes in the Fe_3O_4 film. The FeO areas are so thin that the electrons photoemitted in the Pt substrate can still pass through, while the Fe_3O_4 film is thick enough to completely damp the Pt signal. Considering the electron mean-free path length of about 0.5 nm at the used kinetic electron energy (104.2 eV), one can estimate the thickness of the FeO areas as a few angstroms. Once the Fe_3O_4 film had dewetted and FeO holes were formed, it was not possible to recover a closed Fe_3O_4 film by several additional cycles of Fe deposition and oxidation. Obviously, the Fe atoms adsorbed on the FeO areas at room temperature migrated onto the Fe_3O_4 areas during the oxidation process at 900 K. Consequently, only the Fe_3O_4 grew in thickness, while the FeO zones remained unchanged. Furthermore, wide-range LEEM images of an almost closed Fe_3O_4 film show that FeO domains are formed preferentially at the step bunches of the Pt(111) substrate [Fig 2(f)], where the Fe_3O_4 is unstable, most likely due to the strain induced by the steps and step bunches.

D. Surface inhomogeneities

Besides the two inhomogeneities in the rotational domains and in the morphology discussed so far, we found a third type related to the surface termination. This phenomenon was investigated using four techniques: (i) spot-profile analysis-LEED (SPA-LEED) studying the profile of the LEED spots *in real time*, yielding the domain sizes for different preparations, (ii) XPS of the surface before and after the final annealing,
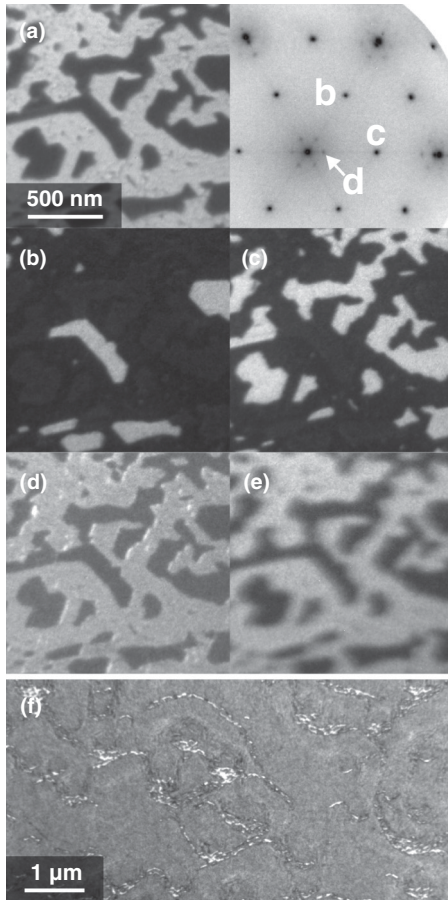
FIG. 2. Strongly dewetted Fe_3O_4 film analyzed by microscopy, diffraction, and local spectroscopy. (a) Bright-field LEEM image ($E_{Kin} = 24$ eV) and corresponding LEED pattern ($E_{Kin} = 88$ eV) showing Fe_3O_4 and FeO structures. The labels in the LEED mark the selected diffraction spots used for the dark-field LEEM images (b), (c), and (d). In (d) facets appear as white lines due to the particular diffraction condition. (e) XPEEM image of the Pt $4f_{7/2}$ photoemission line, $h\nu = 180$ eV, $E_B = 71.6$ eV. (f) Wide-range bright-field LEEM image of a different and almost complete Fe_3O_4 thin film (in gray) with small FeO domains (in white) formed upon the Pt(111) step bunches (the wavy structures still visible in dark gray). $E_{Kin} = 21$ eV.

determining the chemical composition of the surface, (iii) STM of the as-prepared surface, visualizing objects smaller than the LEEM resolution, and (iv) dynamical LEED analysis of the spot intensities for differently prepared surfaces, studying the surface unit cell structure and therefore the termination.

1. Spot-profile-analysis low-energy electron diffraction

The as-prepared, fully closed film oxidized at 1000 K exhibits a shoulderlike broadening around the (0;0) peak [Fig. 3(a)], which gradually disappeared upon a thermal flash to 900 K in UHV. The profile of the specular diffraction spot has been fitted with a superposition of a central peak with a Gaussian-like instrumental broadening and a shoulder that can be described as a sum of three Lorentz$_{3/2}$-like functions of different half widths

$$I_{(00)}(\vec{k}_\parallel, k_\perp) = I_{central}(\vec{k}_\parallel, k_\perp) + I_{shoulder}(\vec{k}_\parallel, k_\perp),$$
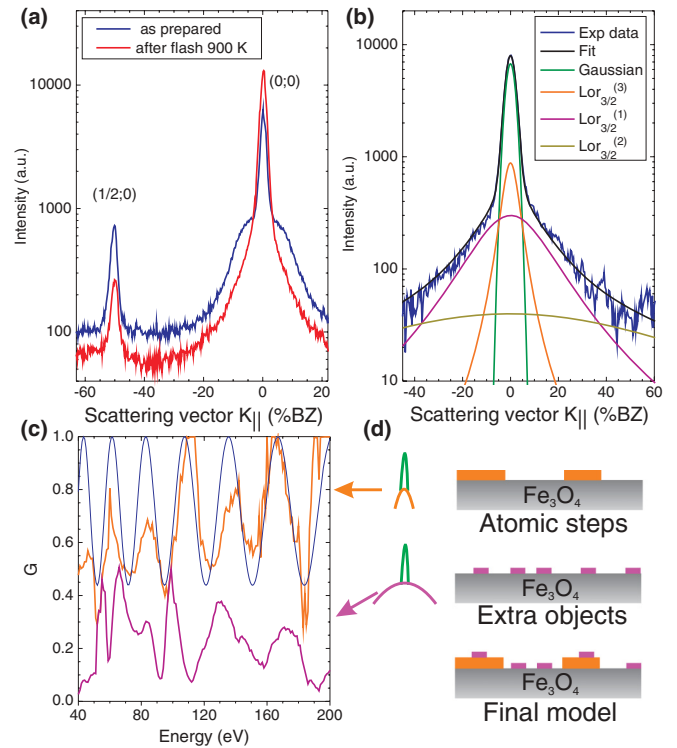

FIG. 3. (Color online) (a) Spot-profile analysis of the LEED pattern for the as-prepared surface (in blue/medium gray) and after a final annealing at 900 K (in red/dark gray). (b) Fit of the LEED profile with a narrow Gaussian for the central peak in green (gray), two Lorentz$_{3/2}$ peaks in orange (light gray), and purple (medium gray) for the shoulderlike broadening and a very broaden Lorentz$_{3/2}$ peak in dark yellow (for the background. (c) Graph of the relative intensities G for the orange (light gray) and purple (medium gray) peaks in function of the energy. The fit for the orange (light gray) curve with $G(S)$ is shown in light blue (light gray). (d) Scheme for the surface model proposed.

with

$$I_{central}(\vec{k}_\parallel, k_\perp) = I_{Gauss}(k_\perp) \cdot f_{Gauss}(\vec{k}_\parallel)$$
$$I_{shoulder}(\vec{k}_\parallel, k_\perp) = I_{Lor3/2}^{(1)}(\vec{k}_\parallel, k_\perp) + I_{Lor3/2}^{(2)}(\vec{k}_\parallel, k_\perp)$$
$$+ I_{Lor3/2}^{(3)}(\vec{k}_\parallel, k_\perp).$$

The prominent broadening, as shown in Fig. 3(b), is described by the first part $I_{Lor3/2}^{(1)}(\vec{k}_\parallel, k_\perp)$. The weakly modulated background, described by the broadened Lorentzian $I_{Lor3/2}^{(2)}(\vec{k}_\parallel, k_\perp)$ with a full width at half maximum (FWHM) as large as the Brillouin zone (BZ), can be related to small clusters of adsorbates on the surface.[26] The third Lorentzian $I_{Lor3/2}^{(3)}(\vec{k}_\parallel, k_\perp)$ has a FWHM slightly larger than the Gaussian one and can be related to the presence of atomic steps. The (0;0) spot profiles have been analyzed in the energy range between 40 and 200 eV. The FWHM for both the central peak and the prominent broadening increases linearly with $k_\perp$; from this behavior a mosaic spread of $\pm 0.2°$ in the Fe_3O_4 film can be calculated, which is much larger than in the Pt substrate (0.007°) determined in the same way. The formation of a mosaic texture is well known for oxide films on metal systems: it has been reported not only for $Fe_3O_4(111)/Pt(111)$[27] but also

for NiO(100)/Ni(100)[28] and NiO and MgO on Ag(100).[29] The mosaic spread was produced during the film preparation and can be caused by small-angle grain boundaries, which might be a compensation mechanism for the lattice misfit between the oxide film and the Pt substrate underneath.

The ratio G between the integral intensities of the $I_{\rm Gauss}$ and $I_{\rm Lor3/2}^{(3)}$ LEED spot components

$$G = I_{\rm Gauss}/\left(I_{\rm Gauss} + I_{\rm Lor3/2}^{(3)}\right)$$

reveals a periodic exchange between two relative intensities [Fig. 3(c)]. G can be modeled by a two-layer system described as

$$G(S,\theta) = 1 - 2\theta(1 - \theta)(1 - \cos(2\pi S)),$$

where $S = k_\perp/(2\pi d)$ is the scattering phase, with $k_\perp$ being the vertical part of the scattering vector $\boldsymbol{k} = \boldsymbol{k}_f - \boldsymbol{k}_i$ and d the step height.[30] Here, the coverage θ is the relative surface area, covered by the second layer. The fit provides a coverage equal to $\theta = 0.17$ ML and a step height value $d = 4.79 \pm 0.09$ Å, fully comparable with the height of the magnetite unit cell (4.85 Å). On the other hand, $G(S,\theta)$ calculated between the Gaussian and the broad $I_{\rm Lor3/2}^{(1)}$ shows no periodicity in $k_\perp$, which is an indication of the presence of objects with a different form factor. From the FWHM, it has been calculated that the objects that generate the predominant broadening have an average lateral size of about 2 nm. Figure 3(d) shows a schematic view of the proposed surface model, which assumes that the distribution of the "atomic steps" causing the third Lorentzian $I_{\rm Lor3/2}^{(3)}(\vec{\boldsymbol{k}}_\parallel,k_\perp)$ is not correlated to the distribution of the "extra objects" related to the first Lorentzian $I_{\rm Lor3/2}^{(1)}(\vec{\boldsymbol{k}}_\parallel,k_\perp)$.

In the following, we investigate and discuss the nature and the origin of the "extra objects." Therefore, the (0;0) LEED spot profiles were analyzed also during the final oxidation and during the subsequent flash at 900 K, to detect the formation, the changes and the disappearance of the shoulder components. It was found that $I_{\rm Lor3/2}^{(1)}$ was not present during the oxidation process when the temperature was still at 1000 K, but it formed during the cooling down at temperature below 750 K. This transient point changed with the cooling rate. Figure 4(a) displays the integral intensities of the sharp central Gaussian and the $I_{\rm Lor3/2}^{(1)}$ components for two different cooling rates, the faster passing from 1000 to 500 K in 120 s (i.e., $\sim$4 K/s—dark lines in the graph) and the slower in 460 s (i.e., $\sim$1 K/s—light lines). For slow cooling rates, the transient occurs even below 670 K. The final shape of the (0;0) spot appeared slightly different for the two cooling rates: the width of the $I_{\rm Lor3/2}^{(1)}$ component decreased from 21% of the BZ for the fast cooling to 10% for the slow cooling, corresponding to twice as large objects when the sample spent more time at lower temperature with O$_2$ exposure. Furthermore, the spot profile was measured when the oxygen exposure was cut off during the cooling process above 750 K. In this case, no broad component $I_{\rm Lor3/2}^{(1)}$ was detected. Therefore, the formation of extra objects on the surface must be directly related to the O$_2$ exposure at lower temperature.

Figure 4(b) shows the intensity behavior during annealing up to 900 K with an average heating rate of 3 K/s. The two oxide films studied were produced with the fast and
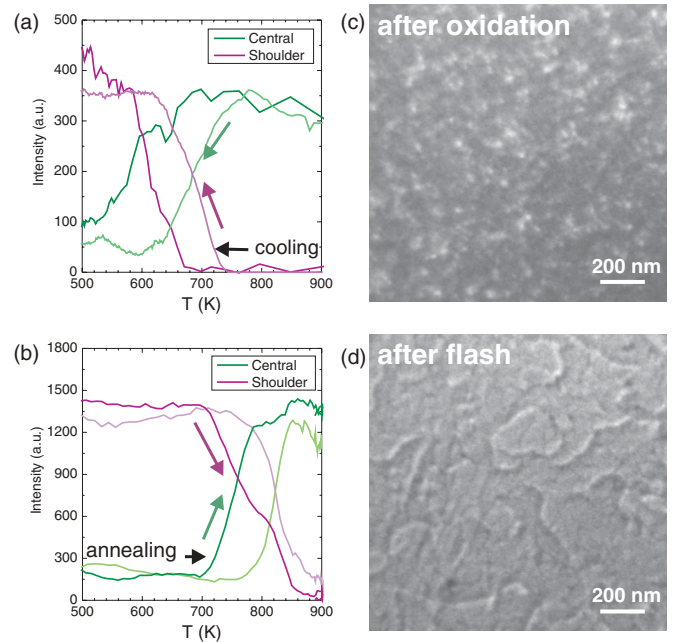
FIG. 4. (Color online) Formation of inhomogeneities during oxidation and annihilation by annealing. (a) Integral intensity of the central Gaussian and the shoulder Lorentz$_{3/2}$ components of the (0;0) LEED spot for fast (in dark) and slow (in light) cooling rate in oxidation atmosphere; $E_{\rm Kin} = 39$ eV. (b) Intensity of the same components during a flash in UHV at 900 K; $E_{\rm Kin} = 39$ eV. (c) and (d) LEEM images of the as-prepared magnetite thin film after the oxidation with slow cooling rate and of the surface after the flash, $E_{\rm Kin} = 24$ eV, with slight overfocus.

slow cooling of Fig. 4(a). The temperature dependence of SPA-LEED during the annealing shows that the objects starts to disappear for temperatures above 700 K for the first cooling and that objects created with slower cooling rate during the oxidation do not disappear below 870 K. Figures 4(c) and 4(d) display typical LEEM images for the as-prepared surface created with the slow cooling rate, before and after the flash, respectively. The as-prepared surface appears very irregular, but well ordered after the flash with terraces of the Fe$_3$O$_4$ film a few 100 nm wide. The roughness of the as-prepared film is due to the oxidation process, which most likely produces dense extra objects smaller than the lateral resolution in the experiment (20 nm) and makes, therefore, the morphology (atomic steps) of the Fe$_3$O$_4$ layer invisible.

2. X-ray photoelectron spectroscopy

Based on the results from SPA-LEED measurements, XPEEM images were taken to check whether the surface inhomogeneity was related to possible contaminations originating from the background pressure (carbon- and nitrogen-related gaseous species) or from possible migration of Mo from the cap that held the sample. From a stack of XPEEM images taken for a defined kinetic energy range and with fixed photon energy, one can extrapolate the XPS spectra from a controlled and localized area of the sample. These spectra were measured both for the as-prepared surface and after the flash at 900 K, with an energy resolution of 0.5 eV. In the spectra no C 1s, N 1s, and Mo 3d core level photoemission lines were detected.
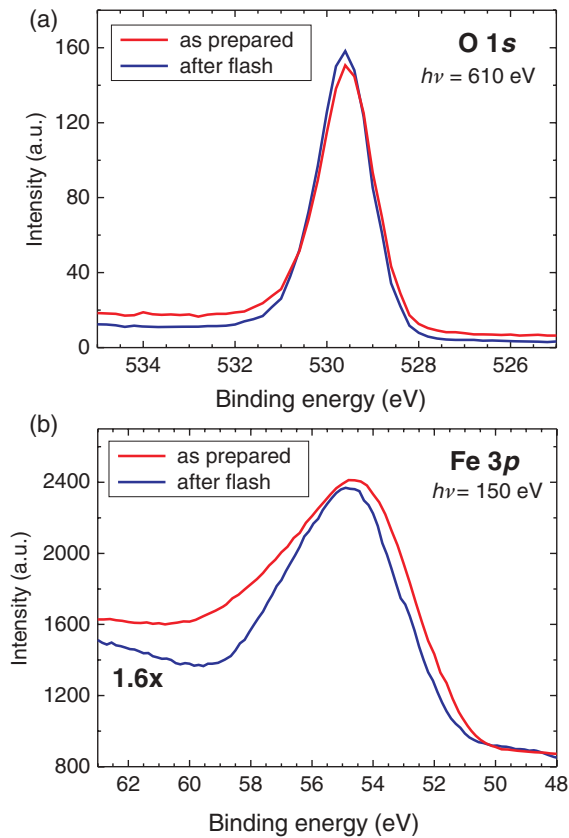
FIG. 5. (Color online) Influence of the final annealing on the extra oxygen-driven species: O 1s (a) and Fe 3p (b) XPS spectra of the as-prepared Fe_3O_4(111) film and after a flash at 900 K.

FIG. 6. (Color online) Typical STM image of an as-prepared Fe_3O_4(111) film. This film was oxidized in 2×10^{-6} mbar O_2 at 1000 K; at the subsequent cooling down the oxygen was pumped out at 500 K. Several species are observed as indicated (see text). Tunneling bias 1.4 V, current 1 nA.

Both the O 1s and the Fe 3p core level spectra (Fig. 5) change during the final flash, whereas the two spectra have been taken within a few minutes without any change of the beamline parameters or of the microscope in between. A fit of the O 1s line with a single Voigt function reveals a small peak shift of 0.10 eV between the two spectra. Due to the limited energy resolution, it is not possible to verify whether the shift is caused by superposition of several components. However, it is a strong indication that the annealing changes the electronic properties of the surface. In XPEEM no image contrast and therefore no further details of the surface were detected. This means that there is no domain of chemical species larger than the lateral resolution in the XPEEM experiments (50 nm).

3. Scanning tunneling microscopy

Figure 6 shows a typical STM image of an as-prepared Fe_3O_4(111) film, which was prepared in a different experimental setup but with the same preparation recipe, including the fast cooling rate described above for the SMART experiment. Several species can be clearly identified on the film surface: triangularly shaped islands (1), randomly distributed broad protrusions (2), and located in registry to the ordered lattice of small protrusion with 6-Å periodicity (3). This periodic structure has been reported in several STM studies of the Fe_3O_4(111) surfaces (both for single crystals and films) and assigned to Fe atoms on the Fe-terminated surface.[10,11,19] Species (2), which are about 1.5 Å in height, have previously
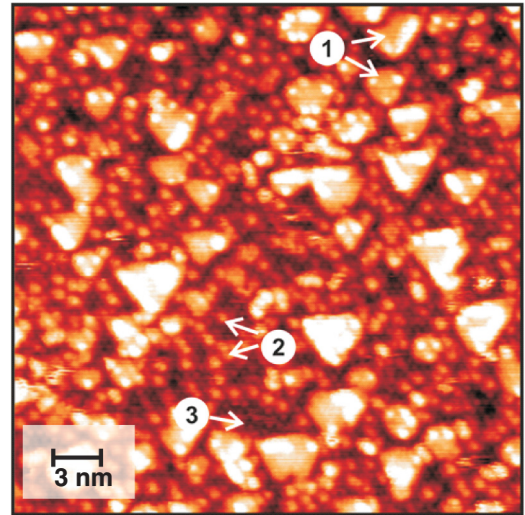
been assigned to adsorbates (presumably water related) as a result of the interaction of the Fe-terminated surface with the residual gases in UHV.[26] This species can explain the weakly modulated background ($I_{Lor3/2}^{(2)}$) detected in SPA-LEED. The flat triangular islands (1) are about 2 nm in average size, and ~2.5 Å in height, with edges running along the main crystallographic directions of the Fe_3O_4(111) surface, which implies a high degree of crystallinity of the island. These islands can be attributed to the broad shoulders $I_{Lor3/2}^{(1)}$ detected in SPA-LEED. In fact, the average size of the triangular-shaped islands (2 nm) is fully compatible with the FWHM of the $I_{Lor3/2}^{(1)}$ component. The islands could not be atomically resolved in our STM experiments, indicating a very low corrugation amplitude, which is anticipated for oxygen-terminated oxide surfaces, where the topmost oxygen layer effectively screens electronic states of underlying metal cations, mainly contributing to the tunneling current.[31] This is in agreement with the SPA-LEED findings, which excludes also that these objects are simply small terraces that present the same atomic termination similar to the rest of the surface: if this would be the case, $G(S)$ should show a periodicity with respect to S, which is in contrast to our experimental results in Sec. III D I.

4. Low-energy electron diffraction (I/V)

We have collected I/V-LEED spectra of the Fe_3O_4 thin film at room temperature before and after the flash at 900 K. The intensity of six different diffraction spots, (0;0), (1/2;0), (0;1/2), (1;0), (0;1), and (1/2;1/2), has been analyzed within an energy range between 40 and 300 eV, equivalent to an overall dataset of 1560 eV. The spectra of each spot have been extracted from recorded LEED patterns via numerical integration over an area large enough to incorporate the signal from the broadening found in the SPA-LEED investigation. The advantages of LEEM systems such as the SMART system
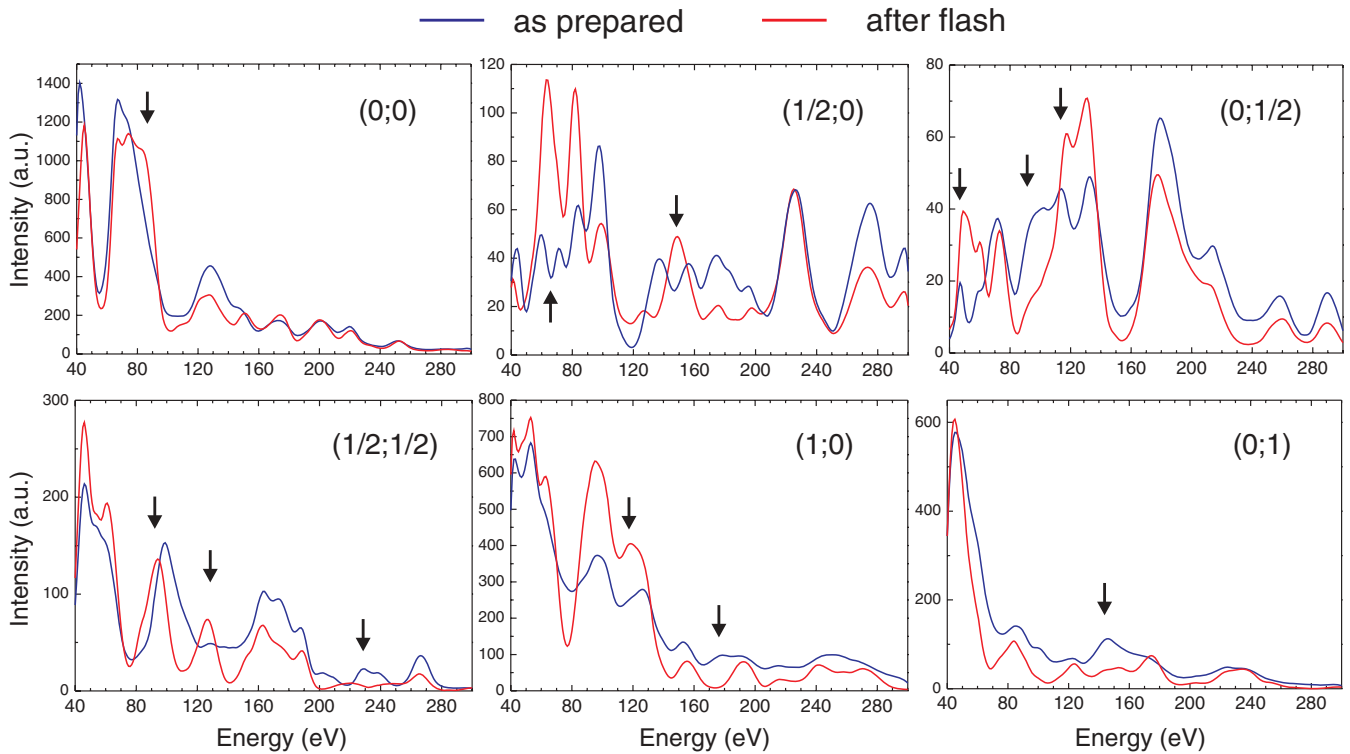
FIG. 7. (Color online) I/V-LEED curves of the first six diffraction spots, for the as-prepared surface and after the annealing at 900 K. The curves have been smoothed via convolution with a Lorentzian function of width equal to 2 eV.[35] The black arrows evidence the major changes produced by the flash.

in collecting these spectra compared to a standard LEED optics are various. During the energy scan, the operation condition of the electron gun and the image columns are not altered, but solely the sample potential is changed. Consequently, the beam current on the sample is constant during the scan, for all experiments. Additionally, due to the optics the investigated diffraction spots do not move in position on the detector during the energy scan, and the (0;0) spot is visible even at full perpendicular illumination. It is also possible to directly inspect the probed surface region from where the diffracted electrons are collected. Combining this with a dark-field image, which gives the portions of the two possible rotational domains, one can easily disentangle the contributions of the two rotational domains and extract the real spectra of (1/2;0), (0;1/2), (1;0), and (0;1) spots of a single rotational domain. This is not possible with a standard back view LEED setup because of the superposition of the two threefold pattern with unknown relative abundance. Therefore, one is forced to average the spectra of spots of the same diffraction order, with consequent loss of information.

In our case the ratio of the two rotational domains was 94%/6%, giving a correction factor of $p = 0.06$, assuming that the experimental LEED pattern is a weighted incoherent superposition of two rotated LEED patterns

$$I_{\text{total}}(\vec{k}_\parallel, k_\perp) = (1 - p)I_+(\vec{k}_\parallel, k_\perp) + pI_-(\vec{k}_\parallel, k_\perp),$$

with the intensity of the two rotational domains $I_+(\vec{k}_\parallel, k_\perp)$ and $I_-(\vec{k}_\parallel, k_\perp)$, and with the probability of $(1-p)$ and p, respec-

tively. Because of the 180° rotation between the domains,

$$I_+(\vec{k}_\parallel, k_\perp) = I_-(\vec{k}_\parallel, k_\perp).$$

As a consequence, one may separate the two contributions as

$$I_+(\vec{k}_\parallel, k_\perp) = \frac{1 - p}{1 - 2p}I_{\text{total}}(\vec{k}_\parallel, k_\perp) - \frac{p}{1 - 2p}I_{\text{total}}(-\vec{k}_\parallel, k_\perp).$$

The resulting disentangled I/V-LEED spectra for the as-prepared and after flash surfaces differ strongly in some energy ranges (see arrows in Fig. 7). This can be interpreted as a change in the surface termination. Additionally, we found that the spectra of the as-prepared surface do not change significantly for different cooling rates.

Our fitting strategy of the I/V spectra was structured in two steps. The first one determined the surface structure of the flashed film assuming its structural homogeneity. Once having obtained this information, we used this structure as a support on top of which small islands, observed as "extra objects" causing the $I_{\text{Lor3/2}}^{(1)}$ broadening in the spot-profile analysis, were placed, in order to fit the I/V data obtained for as-prepared samples. The code we used is Barbieri/Van Hove SATLEED for the generation and the fitting of I/V spectra and for the phase shift calculation; for a detailed computational description of these packages, we recommend a visit to Van Hove's home page.[32] For practical convenience, we describe the Fe$_3$O$_4$ unit cell with the syntax presented in Refs. 7 and 8. The magnetite crystal has a cubic inverse spinel structure that exhibits homonuclear planes along the (111) direction. The structure can be represented by the stacking sequence

$Ba_3Ca_1b_1c_1Ac_3Bc_1a_1b_1C \ldots$ where each letter corresponds to a plane, the subscript number describe the number of atoms in the plane, and the uppercase represents the oxygen atoms. The unit cell defined by the [111] axis (z) together with those axes (x,y) defining the (2×2) structure contains eight oxygen atoms and six iron atoms, organized in four layers. Two closed-packed oxygen layers (four atoms each) stacked in fcc sequence ABCABC are separated by two different iron layers, which alternate in the stacking order. In the first one, called *Kagomé*, three $Fe^{2+,3+}$ atoms populate three quarters of the available octahedrally coordinated sites, situated within a single (111) plane. The second one, called *MixTrigonal*, presents two Fe^{3+} atoms tetrahedrally coordinated and one $Fe^{2+,3+}$ octahedrally coordinated per unit cell; each one has a different z coordinate. With this configuration, one of the four oxygen atoms of the unit cell differs from the other, which presents three bonds toward the Kagomé iron atoms and one to the MixTrigonal, while the others present two bonds toward each iron layer; this induces a slight difference in the position along the z coordinate. For Fe_3O_4 the surface density of a close-packed layer of oxygen represents a monolayer. For the initial configuration of the system, we took those parameters and positions of atoms in the unit cell that are the final result of Ritter and Weiss. The scattering phase shifts were calculated for oxygen and iron atoms in Fe_3O_4 structure up to a maximal quantum number of $l = 7$, assuming a muffin-tin radius of 0.96 Å for O and 0.92 Å for Fe;[33] for the calculation, Debye temperature of 280 K for Fe and 550 K for O were set, and an imaginary part of the inner potential of -5 eV was chosen.[8]

The assumed models for the surface atomic structure were obtained first by truncation of the bulk crystal unit cell along the (111) plane, which yields six different terminations. Additionally, we took into account the possibility that in proximity of the surface, one iron atom can go underneath the first closed-packed oxygen layer, which is suggested as the more energetically favored atomic termination by density functional theory calculations from Zhu *et al.*[34] Also, other more complex structure models were considered, i.e., with incomplete site occupation and/or changed coordination sites. The experimental I/V curves were smoothed via a convolution with a Lorentzian of width equal to 2 eV.[35] Every configuration was optimized until the change in every atomic coordinate in a single iteration loop was below 0.1 Å. Table I (column a) shows the resulting Pendry reliability (R) factors of the relaxed best models. The most reliable model is ¼-ML Fe atom belonging to the MixTrigonal layer on a closed-packed oxygen layer resting upon a Kagomé iron layer. The surface after the flash presents the expected atomic termination. It is important to notice that this is exactly the same result already obtained, first by Barbieri *et al.*[7] and then by Ritter and Weiss.[8]

The fit of the I/V curves measured for as-prepared films gives the results shown in Table I (column b): in general, all R factors are much larger with respect to the values obtained for the flashed surface. The most reliable model was still the one described above for the flashed surface, but with a R factor of 0.33 much worse than before. Assuming that, as shown in the STM images, part of the as-prepared surface exposes the termination dominant after the annealing, one can try to subtract this contribution. The restriction that the resulting

TABLE I. R factors of the I/V-LEED analysis for different models of surface termination in the case of (a) $Fe_3O_4(111)$ surface after a flash at 900 K, (b) $Fe_3O_4(111)$ surface as prepared, and (c) $Fe_3O_4(111)$ surface as prepared with a partial subtraction of the spectra obtained after the flash. The models syntax corresponds to Ref. 7.

Models	R factors		
	a	b	c
$a_1Ba_3Ca_1b_1c_1A$	0.14	0.33	0.50
$Ba_3Ca_1b_1c_1A$	0.23	0.45	0.47
$Ca_1b_1c_1A$	0.53	0.42	0.56
$c_1a_1Ba_3Ca_1b_1c_1A$	0.35	0.48	0.56
$b_1c_1a_1Ba_3Ca_1b_1c_1A$	0.49	0.50	0.54
$a_3Ca_1b_1c_1A$	0.55	0.52	0.65
$c_1Ba_3Ca_1b_1c_1A$	0.37	0.46	0.51
$a_4Ba_3Ca_1b_1c_1A$	0.41	0.44	0.53
$Aa_4Ba_3Ca_1b_1c_1A$	0.79	0.70	1.00
$Ba_4Ca_1b_1c_1A$	0.32	0.44	0.59
$a_1B_3a_3Ca_1b_1c_1A$	0.35	0.40	0.54
$C_3a_1b_1c_1A$	0.58	0.57	0.56

I/V spectra must be greater than zero limits the value of the effective coverage of this termination to $\theta_{eff} = 0.25$ ML. One can, therefore, describe the before flash I/V spectra as a superposition of the intensity after the flash and intensity I_{inh} of the unknown species, i.e.,

$$I_{\text{before flash}}(V) = \theta_{\text{eff}} I_{\text{inh}}(V) + (1 - \theta_{\text{eff}}) I_{\text{after flash}}(V).$$

A new set of spectra of the inhomogeneity $I_{inh}(V)$ has been created

$$I_{\text{inh}}(V) = \frac{1}{\theta_{\text{eff}}} I_{\text{before flash}}(V) - \frac{1 - \theta_{\text{eff}}}{\theta_{\text{eff}}} I_{\text{after flash}}(V).$$

This new set, that represents the I/V spectra of the surface deprived by the contribution of the noncovered surface fraction was now used for the I/V-LEED simulations. The results are shown for $\theta_{eff} = 0.25$ ML in Table I (column c). The R factor of the flashed-surface configuration (top line) rises up to 0.50, while the other models showed no improvement. Also for other θ_{eff} values, we never found an improvement compared to the column in Table I (column b). Therefore, we have to clearly state that all suggested terminations in Table I for the as-prepared surface are not reliable.

IV. DISCUSSION

The comprehensive combination of different microscopic (LEEM, XPEEM, and STM), diffraction (SPA-LEED and I/V-LEED), and spectroscopic (XPS) techniques shed some light on the complex variability induced by changes in the preparation conditions of $Fe_3O_4(111)$ thin films. Following the known recipe,[7] the sample preparation does not result in a completely flat and homogeneous surface but leads to inhomogeneities of different nature. Dark-field LEEM reveals an asymmetry in the distribution of the two rotational domains, with the preference for one of the two domains. This predominance of one domain can be in first order related to the energy required to produce a stacking fault at the interface to the substrate during the formation of the first magnetite layer. The consequent lack of antiphase boundaries (APBs) in

the $Fe_3O_4(111)$ film may, in principle, indicate an anomalous magnetic behavior with respect to the bulk. It is known that in the magnetite thin films, the exchange coupling across APBs is responsible for an unsaturated magnetization even in strong magnetic fields.[24] The fact that the preponderance is preserved after further deposition cycles demonstrates that the asymmetry is already present in the pristine creation of the magnetite film. In the initial phase, the iron deposited on the $FeO(111)$ layer forms $Fe_3O_4(111)$ islands that coalesce into a closed film. Therefore, the orientation of the film domains is a consequence of the orientation of the islands, which is produced by a stacking fault at the $Fe_3O_4(111)/Pt(111)$ interface [the initial $FeO(111)$ layer underneath the islands is converted into $Fe_3O_4(111)$].[27] The substrate could, in this sense, play a crucial role, not only in the determination of the amount of energy required to produce a stacking fault during the pristine formation of the magnetite but also inducing it with the presence of step bunches with a particular alignment that favors one arrangement over the other. Such variability can be of importance for a fine and controlled tuning of the magnetic properties of the thin film.

The morphology of the magnetite thin film is strongly influenced by the temperature at which the oxidation is performed. For films with thickness below 10 nm, an oxidation temperature of 1000 K leads to a dewetting of the film and the formation of holes some hundreds of nanometers wide, which expose a thin FeO layer that covers the Pt substrate. This dewetting can occur even if the magnetite film presents, prior to the oxidation at high temperature, a clear $Fe_3O_4(111)$ LEED pattern with no FeO extra spots. Once formed, the FeO holes remain present even after further cycles of Fe deposition and oxidation. Due to the increasing surface free energy, the polar $FeO(111)$ film cannot be grown thicker than 1 to 2 ML on Pt(111).[19] This generates a supersaturated solution of iron on top of the $FeO(111)$ film. The high mobility at the oxidation temperature lets the iron migrate onto the surrounding $Fe_3O_4(111)$ areas (where the surface free energy is lower) so that Fe does not nucleate in the hole or convert FeO in Fe_3O_4. In this "cleaning" process, the size of the $FeO(111)$ holes plays a crucial role: as long as it is smaller than the depleted zone, the holes will not be filled and converted in $Fe_3O_4(111)$. The Pt substrate morphology has an influence in the formation of the holes: it has been observed that they occur preferentially over the substrate step bunches. Therefore, it is expected that for substrates with high step density (i.e., in case of higher Miller indices), the formation of holes can be enhanced, and a completely closed magnetite film can be obtained only with a careful monitoring of the oxidation temperature.

The surface of the as-prepared sample is populated by objects a few nanometers wide. The formation of these objects at the end of the oxidation process—only during the final cooling in O_2 atmosphere—and the evidence in the XPS spectra that no other contaminants are present in significant quantities lead to the conclusion that they are agglomerates of FeO_x that rest upon the standard terminated Fe_3O_4 surface (1/4-ML Fe over a close-packed oxygen layer) formed before. Although the STM data show that these objects have a regular almost crystalline shape, the I/V-LEED simulations did not lead to a clear model for the termination of the as-prepared surface.

This might be explained by the intrinsic limitation of this kind of analysis. In fact, from the SPA-LEED and the STM results, we know that the investigated objects are on average only 2 nm wide, corresponding to about "7 O atoms"; therefore, they do not fulfill the periodic boundary conditions assumed in the I/V-LEED analysis. On the contrary, these small objects have a large fraction of atoms at the island border with a correspondingly strong scattering contribution. These border atoms are undercoordinated and geometrically shifted with respect to their positions under periodic boundary conditions, which cannot be considered by I/V-LEED simulations. This is also consistent with the change in shape of the O $1s$ and Fe $3p$ XPS spectra, which can be explained by the presence of surface O and Fe atoms with different charge states and coordination. In addition, the assumption of only two terminations coexisting could be too simple: the surface structure might be the result of the superposition of several coexisting metastable terminations, among the one that survives after the flash. However, the presence of FeO_x objects on the surface could, in principle, considerably increase the number and the kind of active sites (for example, undercoordinated Fe atoms of unknown charge state on steps and kinks) for the adsorption of molecules from the residual gas. In general, such objects can also have strong consequences for understanding the catalytic behavior of the $Fe_3O_4(111)$: the local change in stoichiometry might change the reactivity of the whole surface. Furthermore, it can affect the nucleation of metal nanoparticles (with the creation, modification, or inhibition of the nucleation sites) and/or the encapsulation that occurs, for example, in the case of Pt nanoparticles on $Fe_3O_4(111)$.[13] The dynamic LEED analysis confirms that a flat surface with the regular and homogeneous termination according to literature can be obtained only with a flash at 900 K. This may be interpreted as a necessary "cleaning" process inducing migration and desorption of atoms in excess and subsequent rearrangement of the surface toward a homogeneous atomic termination, as well as desorption of oxygen atoms, segregation of iron atoms into the film and exposure of the canonical termination present beneath. In conclusion, the formation of FeO_x agglomerates under certain preparation conditions of the film and their stability at relatively high temperatures can help to sort out the discrepancies in the literature about the magnetite surface termination. Even a slight difference in the preparation conditions (for example, the cooling rate of the system or the final flash performed at temperature below 900 K) can lead to substantial changes in its electronic properties, with important consequences for its behavior in catalysis.

V. CONCLUSIONS

Via the combination of microscopic, spectroscopic, and diffraction techniques, we studied the complex growth of $Fe_3O_4(111)$ on a Pt(111) single-crystal surface, where we examined new surface features and their dependence on preparation conditions. The magnetite thin film exhibits inhomogeneities of a different nature that might influence the chemical and magnetic properties of the surface. The thin Fe_3O_4 film dewets if the initial oxidation is performed at 1000 K, yielding the formation of FeO domains, which are, in fact, holes in the magnetite thin film, preferentially

formed on substrate step bunches. Further deposition of Fe and oxidation does not permit overcoming this inhomogeneity. The analysis of dark-field LEEM images shows a constant predominance of one rotational domain, which could cause an anomalous magnetic behavior with respect to the bulk case. A combined SPA-LEED, XPS, STM, and dynamical LEED study of small surface objects shows that the already observed surface termination (i.e., ¼-ML Fe over a closed oxygen layer) appears only after final annealing at 900 K in UHV. A model that describes a freshly prepared surface predicts the presence of small objects (a few nanometers in size) that partially (below 25%) cover the stable surface. These objects are likely to be weakly ordered FeO_x agglomerates, which can expose atoms with different coordination and charge state compared to the annealed surface. This surface termination is related to the continuous exposure of O_2 during the sample cooling that concludes the oxidation and is influenced by the cooling rate. These agglomerates and their dependence of the preparation conditions add a new complexity to the interpretation of the $Fe_3O_4(111)$ surface termination and its catalytical properties and are an important factor to take into account in comparing existing results.

[1] K. Kochlöfl in *Handbook of Heterogeneous Catalysis*, edited by H. Knözinger, J. Weitkamp, and G. Ertl, Vol. 5, (Wiley-VCH, New York, 1997).

[2] Z. Zhang and S. Satpathy, Phys. Rev. B **44**, 13319 (1991).

[3] M. I. Hirooka, H. Tanaka, R. Li, and T. Kawai, Appl. Phys. Lett. **85**, 1811 (2004).

[4] M. Monti, B. Santos, A. Mascaraque, O. Rodríguez de la Fuente, M. A. Niño, T. O. Menteş, A. Locatelli, K. F. McCarty, J. F. Marco, and J. de la Figuera, Phys. Rev. B **85**, 020404(R) (2012).

[5] W. Weiss and W. Ranke, Prog. Surf. Sci. **70**, 1 (2002).

[6] H. Kuhlenbeck, Sh. Shaikhutdinov, and H.-J. Freund [Chem. Rev. (to be published)].

[7] A. Barbieri, W. Weiss, M. A. Van Hove, and G. A. Somorjai, Surf. Sci. **302**, 259 (1994).

[8] M. Ritter and W. Weiss, Surf. Sci. **432**, 81 (1999).

[9] C. Lemire, R. Meyer, V. E. Henrich, Sh. Shaikhutdinov, and H.-J. Freund, Surf. Sci. **572**, 103 (2004).

[10] N. G. Condon, F. M. Leibsle, T. Parker, A. R. Lennie, D. J. Vaughan, and G. Thornton, Phys. Rev. B **55**, 15885 (1997).

[11] Sh. K. Shaikhutdinov, M. Ritter, X.-G. Wang, H. Over, and W. Weiss, Phys. Rev. B **60**, 11062 (1999).

[12] I. V. Shvets, N. Berdunov, G. Mariotto, and S. Murphy, Europhys. Lett. **63**, 867 (2003).

[13] Z.-H. Qin, M. Lewandowski, Y.-N. Sun, S. Shaikhutdinov, and H.-J. Freund, J. Phys. Chem. C **112**, 10209 (2008).

[14] Y. Joseph, G. Ketteler, C. Kuhrs, W. Ranke, W. Weiss, and R. Schlögl, Phys. Chem. Chem. Phys. **3**, 4141 (2001).

[15] B. Santos, E. Loginova, A. Mascaraque, A. K. Schmid, K. F. McCarty, and J. de la Figuera, J. Phys.: Condens. Matter **21**, 314011 (2009).

[16] R. Fink, M. R. Weiss, E. Umbach, D. Preikszas, H. Rose, R. Spehr, P. Hartel, W. Engel, R. Degenhardt, R. Wichtendahl, H. Kuhlenbeck, W. Erlebach, K. Ihmann, R. Schlögl, H.-J. Freund, A. M. Bradshaw, G. Lilienkamp, Th. Schmidt, E. Bauer, and G. Benner, J. Electron Spectrosc. Relat. Phenom. **84**, 231 (1997).

[17] Th. Schmidt, H. Marchetto, P. L. Lévesque, U. Groh, F. Maier, D. Preikszas, P. Hartel, R. Spehr, G. Lilienkamp, W. Engel, R. Fink, E. Bauer, H. Rose, E. Umbach, and H.-J. Freund, Ultramicroscopy **110**, 1358 (2010).

[18] H.-J. Freund, N. Nilius, T. Risse, S. Schauermann, and Th. Schmidt, Chem. Phys. Chem. **12**, 79 (2011).

[19] W. Weiss and M. Ritter, Phys. Rev. B **59**, 5201 (1999).

[20] Th. Schmidt and E. Bauer, Phys. Rev. B **62**, 15815 (2000).

[21] G. Meyer, M. Michailov, and M. Henzler, Surf. Sci. **202**, 125 (1988).

[22] D. I. Jerdev and B. E. Koel, Surf. Sci. **513**, L391 (2002).

[23] M. Ritter, W. Ranke, and W. Weiss, Phys. Rev. B **57**, 7240 (1998).

[24] D. T. Margulies, F. T. Parker, M. L. Rudee, F. E. Spada, J. N. Chapman, P. R. Aitchison, and A. E. Berkowitz, Phys. Rev. Lett. **79**, 5162 (1997).

[25] A. Sala, Th. Schmidt, and H.-J. Freund (unpublished).

[26] Sh. Shaikhutdinov and W. Weiss, J. Mol. Catal. A: Chem. **158**, 129 (2000).

[27] V. V. Roddatis, D. S. Su, C. Kuhrs, W. Ranke, and R. Schlögl, Thin Solid Films **396**, 78 (2001).

[28] M. Bäumer, D. Cappus, H. Kuhlenbeck, H.-J. Freund, G. Wilhelmi, A. Brodde, and H. Neddermeyer, Surf. Sci. **253**, 116 (1991).

[29] J. Wollschläger, D. Erdös, H. Goldbach, R. Höpken, and K. M. Schröder, Thin Solid Films **400**, 1 (2001).

[30] J. Wollschläger and M. Henzler, Phys. Rev. B **39**, 6052 (1989).

[31] Sh. K. Shaikhutdinov and W. Weiss, Surf. Sci. **432**, L627 (1999).

[32] M. A. Van Hove, http://www.ap.cityu.edu.hk/personal-website/Van-Hove_files/leed/leedpack.html.

[33] R. Pentcheva, W. Moritz, J. Rundgren, S. Frank, D. Schrupp, and M. Scheffler, Surf. Sci. **602**, 1299 (2008).

[34] L. Zhu, K. L. Yao, and Z. L. Liu, Phys. Rev. B **74**, 035409 (2006).

[35] J. B. Pendry, J. Phys. C **13**, 937 (1980).